# Finite element stress analysis of reinforced high-strength concrete columns in severe fires

J.H. Chung*, G.R. Consolazio, M.C. McVay

*Department of Civil & Coastal Engineering, University of Florida, 365 Well Hall, PO Box 116580, Gainesville, FL 32611, USA*

**Abstract**

A finite element stress analysis model is presented that has been developed for numerical prediction of stress states in a reinforced concrete structural element exposed to rapid heating. Using a computational methodology presented to analyze stress states associated with coupled hydro-thermal behavior of concrete exposed to severe fire conditions, multidimensional finite element models that characterize structural response of reinforced concrete columns exposed to radiant heating conditions are developed. Effects of steel reinforcements on coupled heat and moisture transport phenomena are also considered.

*Keywords:* Thermal stress; Temperature; Moisture; Concrete; Fire

## 1. Introduction

In the past, explosive spalling of reinforced concrete (R/C) structures has been investigated by making use of numerical models that analyze mass and heat transfer phenomena in plain concrete exposed to fire. Thermal spalling of intensively heated concrete would result from pore pressure and thermal stress development in concrete structural elements. However, only a limited number of computational analyses that considered hydro-thermal behavior of concrete at high temperatures have been recently reported [1,2]. Consequently, very few simulation codes that are capable of simulating the coupled hydro-thermal *and* structural behavior of concrete structures have been developed in this research field. The need for development of a new numerical tool capable of simulating such coupled processes is thus evident.

A goal of this paper is to numerically quantify such effects and to evaluate their influence on thermally induced stresses of three-dimensional R/C structures subjected to rapid heating. In order to accomplish this goal, implementation of a new analytical model is accomplished by adding thermal modeling features to the existing PLASFEM nonlinear finite element code [3]. To conduct the present study, a three-dimensional combined finite difference and finite element model has been developed that is capable of analyzing transient heat conduction in partially saturated concrete and predicting states of effective stress.

## 2. Model description

A square cross-section (380 mm × 380 mm) reinforced concrete column exposed to a radiant fire condition shown in Fig. 1 is modeled. All four sides of the column are exposed to a hydrocarbon pool fire (modeled by ASTM E1529 [4]). The longitudinal bars are no. 6 bars and ties of no. 3 bars are provided to serve as shear reinforcement for the reinforced concrete column. Vertical spacing of ties used in the model is 40 mm. The ends of the ties are lap sliced with corner hooks that are idealized as perfectly anchored by a 90° bend around a bar. Confining effects in the concrete core and interface between the longitudinal bars and the ties are not considered in the finite element analysis. More importantly, the effects of steel reinforcement on hydrothermal behavior of concrete are considered in order to quantify the influence of R/C structural element heterogeneity on thermodynamic state development and thus, the influence on development of thermally induced stress field.

Using symmetry of the geometry and the thermal loading conditions, a partial symmetry model of the column segment is developed (Fig. 2) as a single

* Corresponding author. Tel.: +1(352) 392 9537 ext 1495; Fax +1(352) 392 3394; E-mail: jchun@ce.ufl.edu


*Computational Fluid and Solid Mechanics 2005*
K.J. Bathe (Editor)

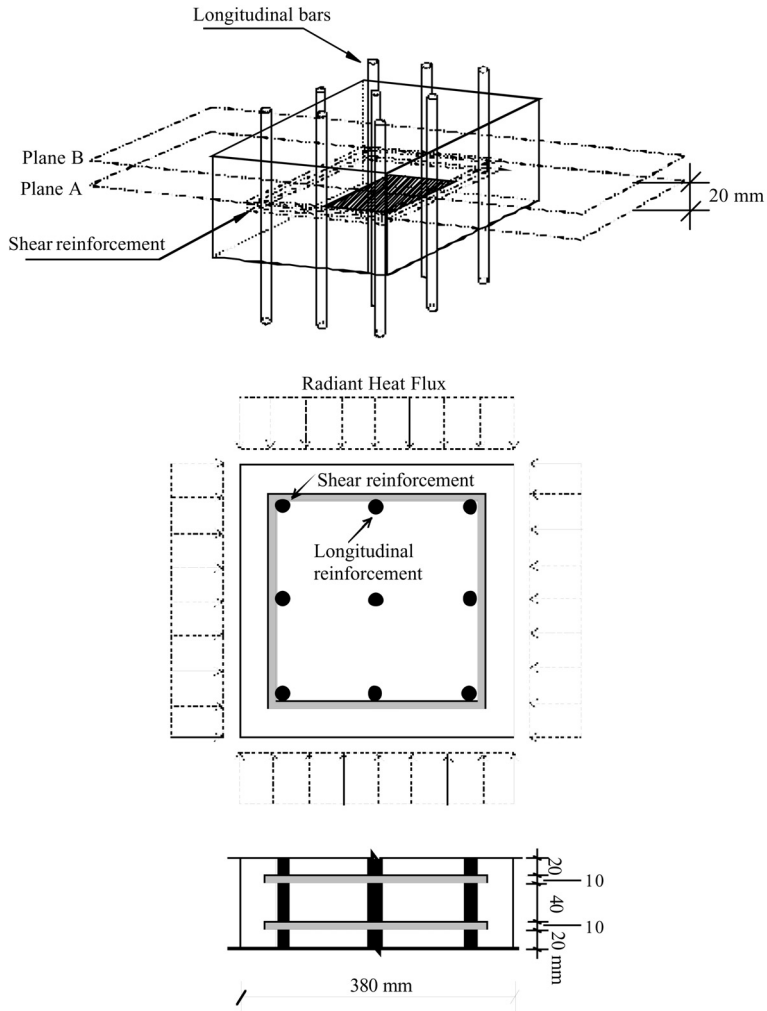


Fig. 1. A reinforced concrete column exposed to radiant heat.

quadrant mesh symmetric in both the *xz*- and the *xy*-plane. Figures 2(a) and (b) illustrate the finite element mesh layout in plane views at $y = 2.5$ mm and y = 20.0 mm, respectively. In subsequent discussion, the plane view shown in Fig. 2(a) is referred to as Plane A while the one shown in Fig. 2(b) is referred to as Plane B.

Two different sets of boundary conditions that bracket realistic field conditions (e.g. material constraint) are considered. In the first case, vertical expansion is completely restrained (Fig. 2(c)), while in the second the top of the column segment is free to expand (Fig. 2(d)). At a plane of geometric symmetry, mechanical displacement boundary conditions for the symmetric thermal loading are modeled such that no translational motion is allowed perpendicular to a plane of geometric symmetry.

## 3. Modeling of transient thermal loading conditions

Solving the coupled heat and moisture flow equations yields a complete three-dimensional time-varying description of the temperature field throughout three-dimensional directions of the column [5]. Temperature data (Figs. 3 and 4) obtained from the three-dimensional finite difference model is then mapped onto nodes located in the finite element thermal stress models that were meshed using a 27/8 element formulation [6]. In this formulation, lower-order temperature interpolations, e.g. first-order polynomial functions, have been used as the finite basis functions for nodal temperature degrees of freedom, but higher-order displacement interpolations, e.g. second-order polynomial functions, have been used for nodal displacement degrees of freedom.

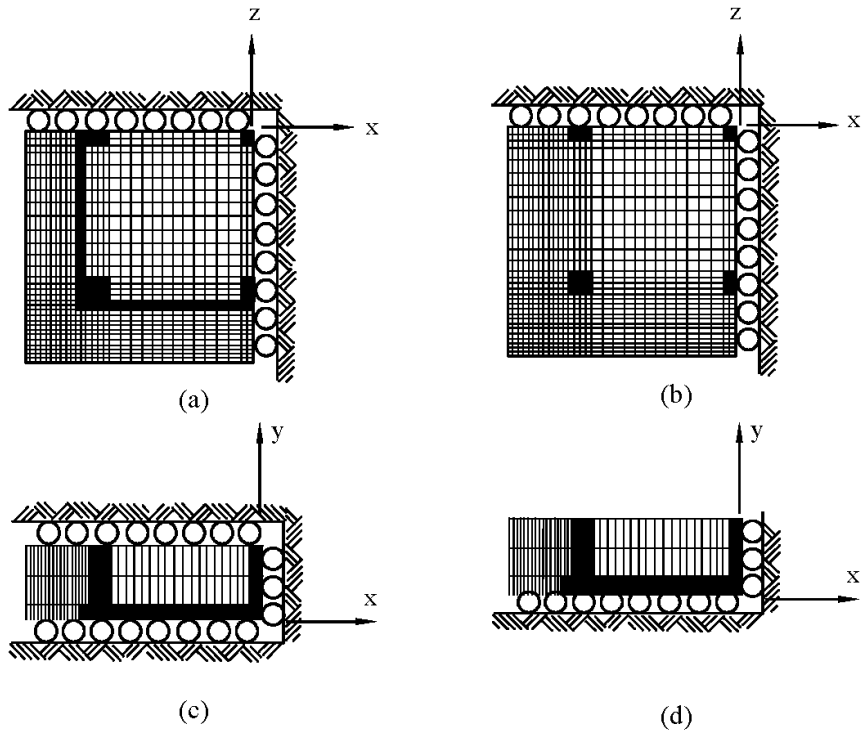


Fig. 2. Three-dimensional finite element models of the concrete column segment.

For each finite element model nodal point, a complete time-history of temperature is extracted from the finite difference simulation results and is then applied to the finite element model as a time varying prescribed nodal temperature $\{T_a^{prescribed}\}$. Time-varying thermal stress analyses are then performed for each boundary condition model to compute time-histories of thermal stresses throughout the three-dimensional meshes. At each time step, the following system equation is solved:

$$[K_u]\{d\}_{n+1} = \{F_T\}_{n+1} \tag{1}$$

where $[K_u]$ is the mechanical stiffness matrix, $\{d\}_{n+1}$ denotes the global mechanical displacement vector at time $t_{n+1}$, and $\{F_T\}_{n+1}$ represents the thermally induced force vector

$$\{F_T\}_{n+1} = \int_V [B]^T \{\beta\} [\hat{N}]\, d\Omega \cdot \{T_a^{prescribed}\}_{n+1} \tag{2}$$

where $[B]$ is the strain-displacement matrix, $[\hat{N}]$ is the mapping function matrix for nodal temperature degrees of freedom, and the thermo-mechanical coupling matrix $\{\boldsymbol{\beta}\}$ is defined as $\{\boldsymbol{\beta}\} = -3K\boldsymbol{\alpha}\cdot\{1\ 1\ 1\ 0\ 0\ 0\}^T$. $K$ and $\boldsymbol{\alpha}$ represent the bulk modulus and the linear thermal expansion coefficient, respectively. We compute thermal stresses at time $t_{n+1}$ through the generalized Hooke's law

$$\{\boldsymbol{\sigma}\}_{n+1} = [C]\{\boldsymbol{\varepsilon}\}_n - \{\boldsymbol{\beta}\}\boldsymbol{\Delta} T_{n+1} \tag{3}$$

where $[C]$ is an elasticity-coefficient matrix, $\{\epsilon\}_n = [B]\{d\}_n$, and $\Delta T_{n+1}$ is the temperature change at a point of interest in the natural coordinate system denoted by $r$, $s$, and $t$, given by

$$\Delta T_{n+1}(r,s,t) = \sum_{i=1}^{8} \hat{N}_i(r_i, s_i, t_i) \cdot \left( (T_i^{prescribed})_{n+1} - (T_i^{prescribed})_n \right) \tag{4}$$

Changes in material temperature due to mechanical strain are assumed to be negligibly small and can therefore be neglected. Mechanical properties of a typical high strength concrete and structural steel are collected from field tests reported in [7].

## 4. The principle of stress superposition

To analyze the combined effects of moisture movement and temperature gradient development in the computation of thermally induced stresses, the principle of superposition is used in solving the linear momentum balance equation with mixed boundary conditions. Using the *volume fraction* term $\eta_\pi(\pi = s, w, g$; solid, liquid water, and gas respectively) and assuming that

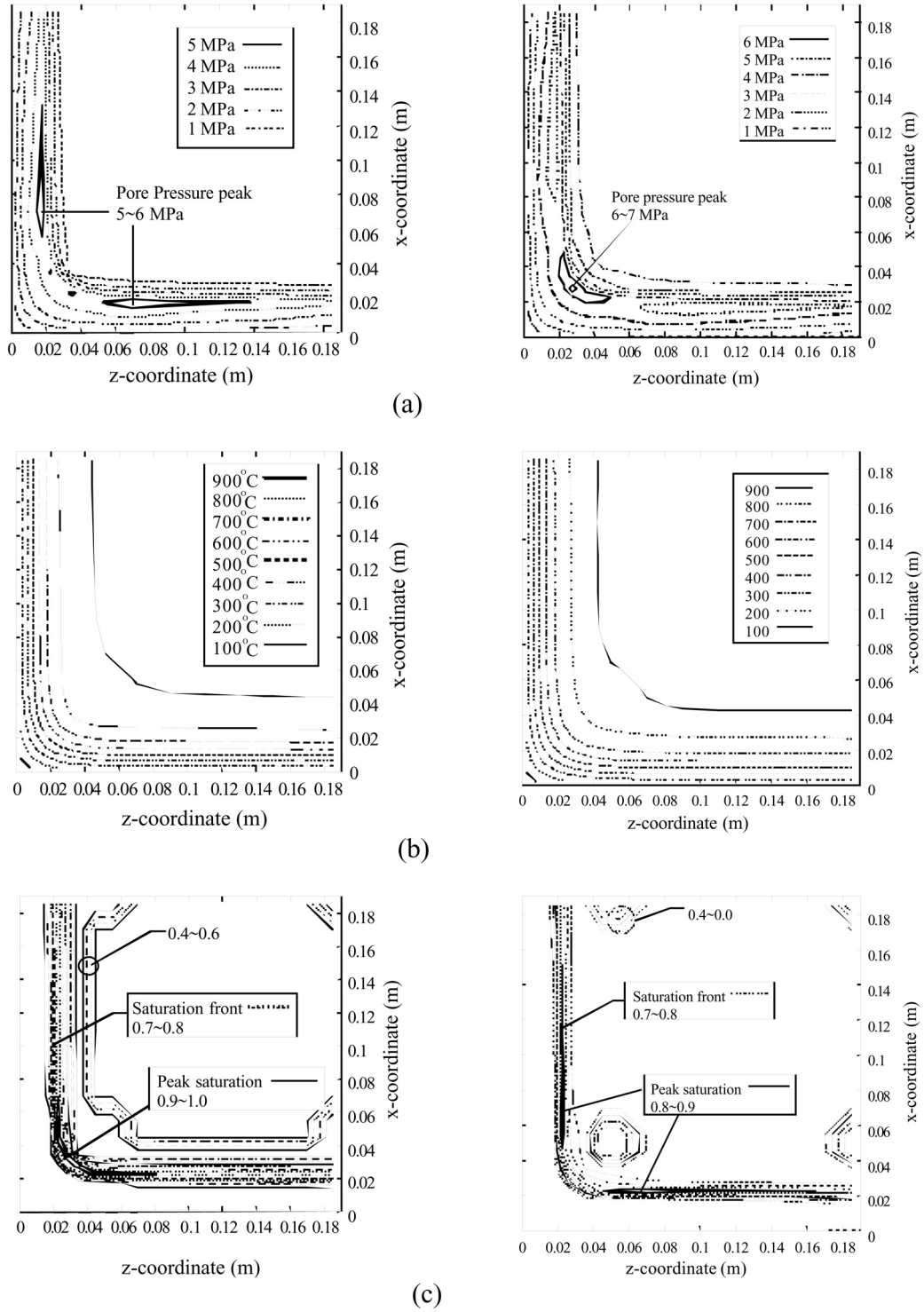


Fig. 3. Thermodynamic states at t = 600 s. (Data plotted for a square column segment Plane-A (left column) and Plane-B (right column) of Figure 2). (a) Pore Pressure, (b) temperature, (c) saturation.

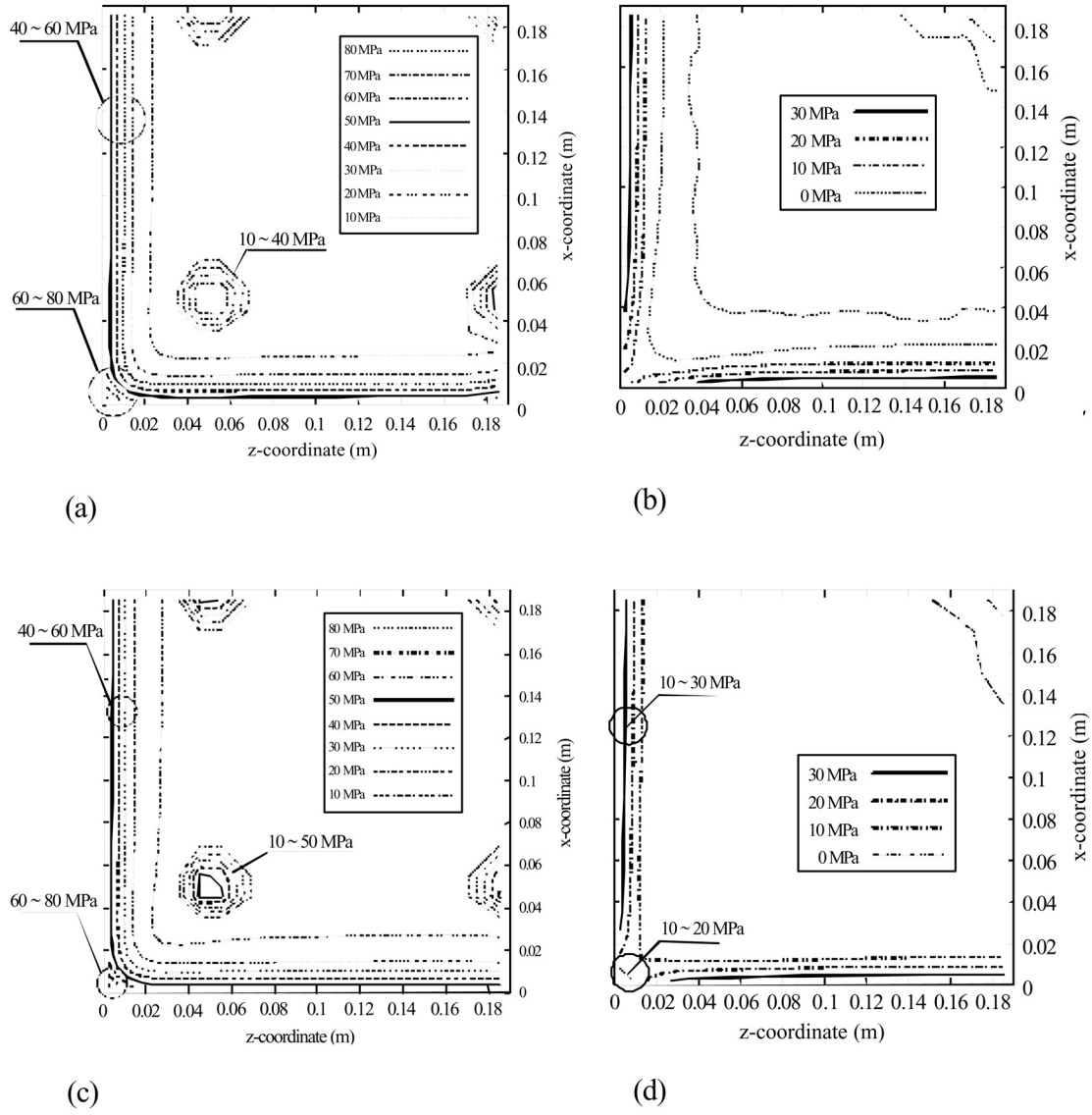


Fig. 4. Maximum principal stresses at t = 600 s. (a) Stress contour in Plane A (fixed boundary), (b) stress contour in Plane A (free boundary), (c) stress contour in Plane B (fixed boundary), (d) stress contour in Plane B (free boundary).

shear stresses in fluid phases (liquid water and the air–water vapor mixture) are negligible and local thermodynamic equilibrium exists, then $p_w = p_g = p$ where $p$ is the internal pore pressure (obtained from finite difference analyses), and the total stress tensor may be expressed as

$$\underset{\sim}{\sigma} = \underset{\sim}{\sigma}''_s - n_p \cdot p\underline{\underline{I}} \tag{5}$$

where $\underset{\sim}{\sigma}''_s$ is the effective stress acting on the solid skeleton and $n_p$ is the boundary porosity [7].

## 5. Simulation results

Figures 4(a) and (c) show maximum principal stresses $\sigma_1$ developed in the case of a fully constrained boundary condition imposed on $y$-direction displacements shown in Fig. 2(c). This case will be referred to as the fixed boundary condition case. Owing to large effective tensile stresses acting normal to the $xz$-plane, i.e. $\sigma''_{yy}$, the severe maximum principal stresses acting on the principal $xz$-plane are developed in the concrete cover zone of the column segment. One particularly noteworthy

feature of the thermally induced stress field is severe development of effective tensile stress $\sigma''_{yy}$ in the near-surface regions along the surface of the column segment and in the near-corner regions.

Figures 4(b) and 4(d) show maximum principal stresses $\sigma_1$ developed in the case of no constraint imposed on the top boundary of the column segment (Fig. 2(d)). In contrast to the fixed boundary condition case, maximum tensile stress components of the effective stress tensor computed in the near-surface regions are $\sigma''_{xx}$ and $\sigma''_{zz}$ rather than $\sigma''_{yy}$. Thus, large effective tensile stresses are developed perpendicular to the $yz$-plane, i.e. $\sigma''_{xx}$, and mainly contribute to the maximum principal stress in the surface region acting in the x-direction. However, acting perpendicular to the $xy$-plane, $\sigma''_{zz}$ is found to be the dominant tensile stress component along the $z$-coordinate. This reveals that characteristics of the stress field developed in the free boundary condition case such that the development of dominant tensile stress component is direction-dependent but results in the development of large maximum principal stresses in the surface regions.

## 6. Conclusion

The effects of moisture on temporal temperature distributions result in significant changes of thermally induced stress field. Temperature distribution changes and high pore-pressure are affected by impermeable reinforcing steel in the concrete and result in severe thermally induced stresses in near-surface regions of a reinforced concrete column. The magnitudes of thermally induced stresses at t = 600 s after all four sides of the column exposed to fire, ranging from 30 MPa (4.4 ksi) to 80 MPa (11.6 ksi), could well exceed typical tensile strengths of high-strength concrete.

## References

[1] Tenchev RT, Li LY, Purkiss JA, Khalafallah BH. Finite element analysis of coupled heat and mass transfer when it is in fire. Magazine of Concrete Research 2001;53(2):117–125.

[2] Chung JH, Consolazio GR. Moisture movement and heat flow in reinforced concrete columns exposed to fire. In: Bathe KJ, editor, Proc of 2nd MIT Conference on Computational Fluid and Solid Mechanics. Oxford: Elsevier Science, 2003.

[3] McVay MC, Geotechnical Numerical Group. PLASFEM Version 2.4 Manual. Department of Civil and Coastal Engineering, University of Florida, 1998.

[4] ASTM. Standard Test Methods for Determining Effects of Large Hydrocarbon Pool Fires on Structural Members and Assemblies. ASTM E 1529–93, American Society for Testing and Materials, PA, USA, 1993.

[5] Chung JH, Consolazio GR. Numerical modeling of transport phenomena in reinforced concrete exposed to elevated temperatures. Cement and Concrete Res 2005 (to appear).

[6] Bathe KJ. Finite Element Procedures. Englewood Cliffs, NJ: Prentice Hall, 1996.

[7] Bažant ZP, Kaplan MF. Concrete at High Temperatures: Material Properties and Mathematical Modeling. Harlow, UK: Longman Group Limited, 1996.